Journal of Alloys and Compounds 509 (2011) 891–898

Contents lists available at ScienceDirect

Journal of Alloys and Compounds

journal homepage: www.elsevier.com/locate/jallcom

Joining mechanism of Ti/Al dissimilar alloys during laser welding-brazing process

Shuhai Chen[a,b,*], Liqun Li[b], Yanbin Chen[b], Jihua Huang[a]

[a] School of Materials Science and Engineering, University of Science and Technology Beijing, Beijing 100083, PR China
[b] State Key Laboratory of Advanced Welding Production Technology, Harbin Institute of Technology, Harbin 150001, PR China

ARTICLE INFO

Article history:
Received 8 July 2010
Received in revised form
22 September 2010
Accepted 22 September 2010
Available online 29 September 2010

Keywords:
Laser welding–brazing
Joining mechanism
Ti/Al dissimilar alloys
Stacking fault

ABSTRACT

Joining mechanism of Ti/Al dissimilar alloys was investigated during laser welding–brazing process with automated wire feed. The microstructures of fusion welding and brazing zones were analysed in details by transmission electron microscope (TEM). It was found that microstructures of fusion welding zone consist of α-Al grains and ternary near-eutectic structure with α-Al, Si and Mg_2Si. Interfacial reaction layers of brazing joint were composed of α-Ti, nanosize granular $Ti_7Al_5Si_{12}$ and serration-shaped $TiAl_3$. For the first time, apparent stacking fault structure in intermetallic phase $TiAl_3$ was found when the thickness of the reaction layer was very thin (approximately less than 1 μm). Furthermore, crystallization behavior of fusion zone and mechanism of interfacial reaction were discussed in details.

1. Introduction

In aeronautic and automotive industries, weight reduction is strongly demanded for energy and natural resource savings. The joining of dissimilar alloys is one of the effective measures to reduce weight of the structures or save rare metal, such as joining of Ti/Al [1–3], Cu/Al [4–6], Fe/Al [7,8]. Among above partners, hybrid structure of Ti/Al dissimilar alloys is an attractive design for the weight reduction and some local requirements. However, thermal joining of aluminum and titanium has a metallurgical challenge due to unavoidable formation of brittle intermetallic compounds [9–13]. Therefore, it is necessary to control effectively formation and growth of Ti–Al intermetallic compounds.

In order to suppress the growth of the brittle intermetallic phase, explosive welding [14], diffusion–bonding [3,9] and brazing [15] have been widely used to join aluminum to titanium. However, these methods are not suitable for joining tailored blanks and flexible manufacture due to the limitation of especial joint configuration or whole heating. In recent years, friction stir welding was attempted to weld aluminum and titanium [16]. However, the maximum failure load of the joint is only about 62% that of Al alloy base metal and needs further improvement.

As a heat source of materials processing, laser has been widely applied in the fields of welding [17] and cladding [18,19]. In the joining of dissimilar alloys, laser welding method provides some advantages such as high energy density, rapid heating/cooling velocity and accessibility to the heating zone [20,21]. Specially, the laser welding–brazing method to attach metallurgical non-fitting partners to each other can suppress effectively the growth of brittle intermetallic compounds [22–25]. Hence, tensile strength of the joint by laser welding–brazing was enhanced significantly. In addition, this method provides good adaptability and a good relation between weight reduction and costs in serial production.

In our study [26–28], circular and rectangular spot laser welding–brazing processes of Ti/Al dissimilar alloys was developed, while V-shaped groove with 45° angle was fabricated on parent materials. The thickness of brittle reaction layer could be limited to the level of just a few microns under the condition of appropriate process parameter (laser power 2400 W, offset of laser beam to Al 0.4 mm, welding speed 0.8 m/min, wire feed rate 3.2 m/min), and the tensile strength of the joints is up to 290 MPa, which exceeds 80% that of Al alloy base metal. In general, thermal cycle of laser welding–brazing have characteristics of high peak temperature, high heating/cooling velocity and short interaction time between liquid filler and solid base metals. So in such environment of far from equilibrium, interfacial reaction mechanism has novel interesting characteristic. Expounding the process has significant to control mechanical property of joint, as well as to guide composition design of welding materials. In addition, it is important to describe crystallization behavior of the fusion zone, which will influence on appearance and mechanical properties of the joint.

This study focused on joining mechanism of Ti/Al dissimilar alloys during laser welding–brazing process. Crystallization behavior of the fusion zone, element diffusion behavior and growth

* Corresponding author at: School of Materials Science and Engineering, University of Science and Technology Beijing, 30 Xueyuan Road, Haidian District, Beijing100083, PR China. Tel.: +86 010 62334859.
E-mail address: shchenhit@gmail.com (S. Chen).

0925-8388/$ – see front matter © 2010 Elsevier B.V. All rights reserved.
doi:10.1016/j.jallcom.2010.09.125

Table 1
Compositions of 5A06 Al, Ti–6Al–4V alloy and filler metal used in this study.

Alloys	Elements (wt.%)												
	Al	Ti	Mg	Si	Cu	Mn	Fe	Zn	V	C	N	H	O
5A06	Bal.	0.02	5.8–6.8	0.4	0.1	0.5–0.8	0.4	0.2	–	–	–	–	–
Ti–6Al–4V	5.5–6.8	Bal.	–	–	–	–	0.3	–	3.5–4.5	0.1	0.05	0.01	0.2
Filler wire	Bal.	0.15	0.1	12.0	0.3	0.15	0.8	0.2	–	–	–	–	–

mechanism of interfacial intermetallic compounds were discussed based on detailed microstructure analysis.

2. Experimental details

Ti–6Al–4V alloy and 5A06 Al alloy plates with thickness of 1.5 mm were selected as the laser joining materials. In this study, flux-cored wire with the diameter of 2 mm was used as filler materials. The compositions of parent metal and filler wire are listed in Table 1.

Non-uniform heating and small heating area are disadvantages to melt stably filler wire and wet base metals. Therefore, the laser beam was modulated to a rectangular spot (focal spot size 2 mm × 4 mm) by the integral mirror to get relatively uniform energy distribution. To further improve the spreadability, the V-shape groove with 45° angle was fabricated on base metals. Double shielding argon gas was used at double sides of workpieces to avoid oxidation of liquid metals. The laser beam irradiated vertically on the surface of workpiece, and there was a focal spot position at the top surface of the workpiece during laser welding–brazing process. The angle of the filler wire and the workpiece was adjusted to 30°. Filler wire was fed at the front of the laser beam, as illustrated in Fig. 1. To decrease differences of heat conductivity and reflectance of Ti and Al, the offset of laser beam toward Al base metal was 0.4 mm.

In this research, the microstructure of joints was observed by optical microscope (OM) and scanning electron microscope (SEM) equipped with an energy-dispersive X-ray spectrometer (EDS) after standard grinding and polishing procedures and etching with mixed solution (1 vol.% HF + 1.5 vol.% HCl + 2.5 vol.% HNO_3 + 95 vol.% H_2O). Transmission electron microscopy (TEM) with a Philips CM12, operating at 120 kV, was used to characterize the microstructure in details.

Specimens for transmission electron microscopy (TEM) were prepared with cutting, grinding and ion milling to electron transparency. Thin sheets (5 mm × 8 mm × 0.2 mm) were cut from brazing zone where the interface reaction zone was approximately located in midline and fusion welding zone by a linear cutting machine. The thin sheets were thinned down into parallel sided and semi-thin sheets with thicknesses of around 40 μm through several steps of coarse grinding, fine grinding and mechanical polishing. The semi-thin sheets were then cut into 3 mm discs. Ion milling was performed on both sides of the specimens with two beams of 4 kV Ar ions by using a Gatan 691 Ion-Miller. It should be pointed out that the preparation of specimens for brazing zone was very difficult to obtain electron transparency at reaction layer due to positional uncertainty of Ar ions bombardment. After repeated attempts the specimens with electron transparency at reaction layer have been achieved.

3. Results

Macroscopic cross section of the Ti/Al dissimilar joint by laser welding–brazing is shown in Fig. 2. In the laser welding–brazing process, Al alloy composed about of 6% (wt.) Mg and filler wire composed of eutectic composition of Al and Si were melted and mixed under irradiation of laser beam. Consequently, a fusion welding zone with hypoeutectic microstructure was formed in the one side. At the same time, Ti alloy in solid state interacted with liquid mixed metal, and a brazing zone was formed in the other side. Therefore, laser welding–brazing joint has dual characteristics of fusion welding and brazing. The formation of intermetallic compounds could be suppressed effectively by this method, and so mechanical property of joint was enhanced markedly. These results had been described in detail elsewhere [26,28]. In the following parts, we will analyse the microstructures of fusion welding and brazing zone.

3.1. Microstructure of fusion zone

Fig. 3 shows the microstructure of fusion zone magnified in Fig. 2 marked with rectangles A and B, as shown in Fig. 3(a). There were four different zones: parent metal (PM), fusion line (FL), columnar crystal zone (CCZ), equiaxed crystal zone (ECZ). Fig. 3(c) presents fine hypoeutectic microstructure of fusion zone magnified in Fig. 3(a) marked with rectangle C. The microstructures in CCZ and ECZ are similar to that in FL as partial melting Al alloy mixed with the completely melting filler wire. The CCZ contains coarse columnar α-Al solid grains and near-eutectic structures between neighbouring α-Al grains. The coarse columnar structure was nearly vertical to the fusion line, which was induced by the higher cooling rate and the preferential direction of the thermal conduction. In addition, microstructure morphology of fusion zone near Ti alloy is the vertical to the interface. However, there is no significance compared with microstructure morphology of adjacent Al alloy, as shown in Fig. 3(b).

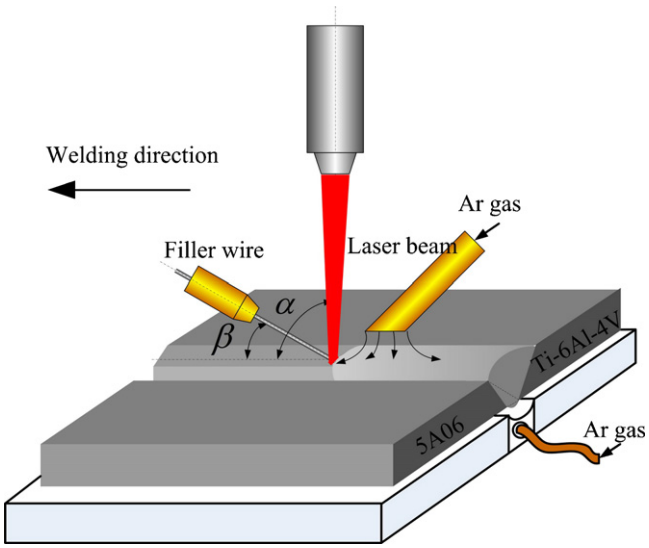

Fig. 1. Schematic drawing of the laser welding–brazing processing.

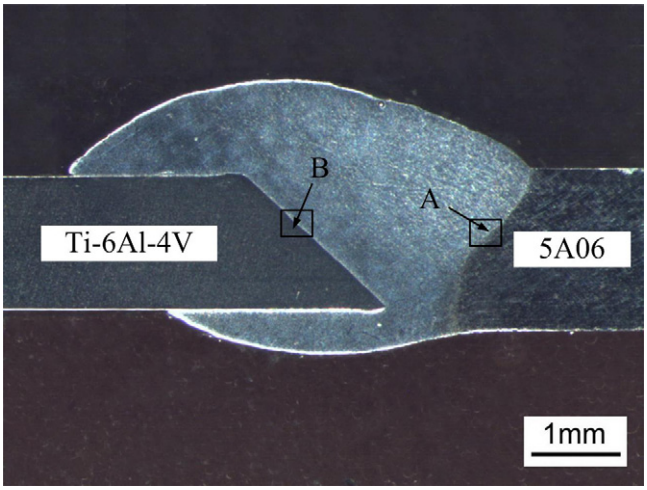

Fig. 2. Macroscopic cross section of the joint by laser welding–brazing.

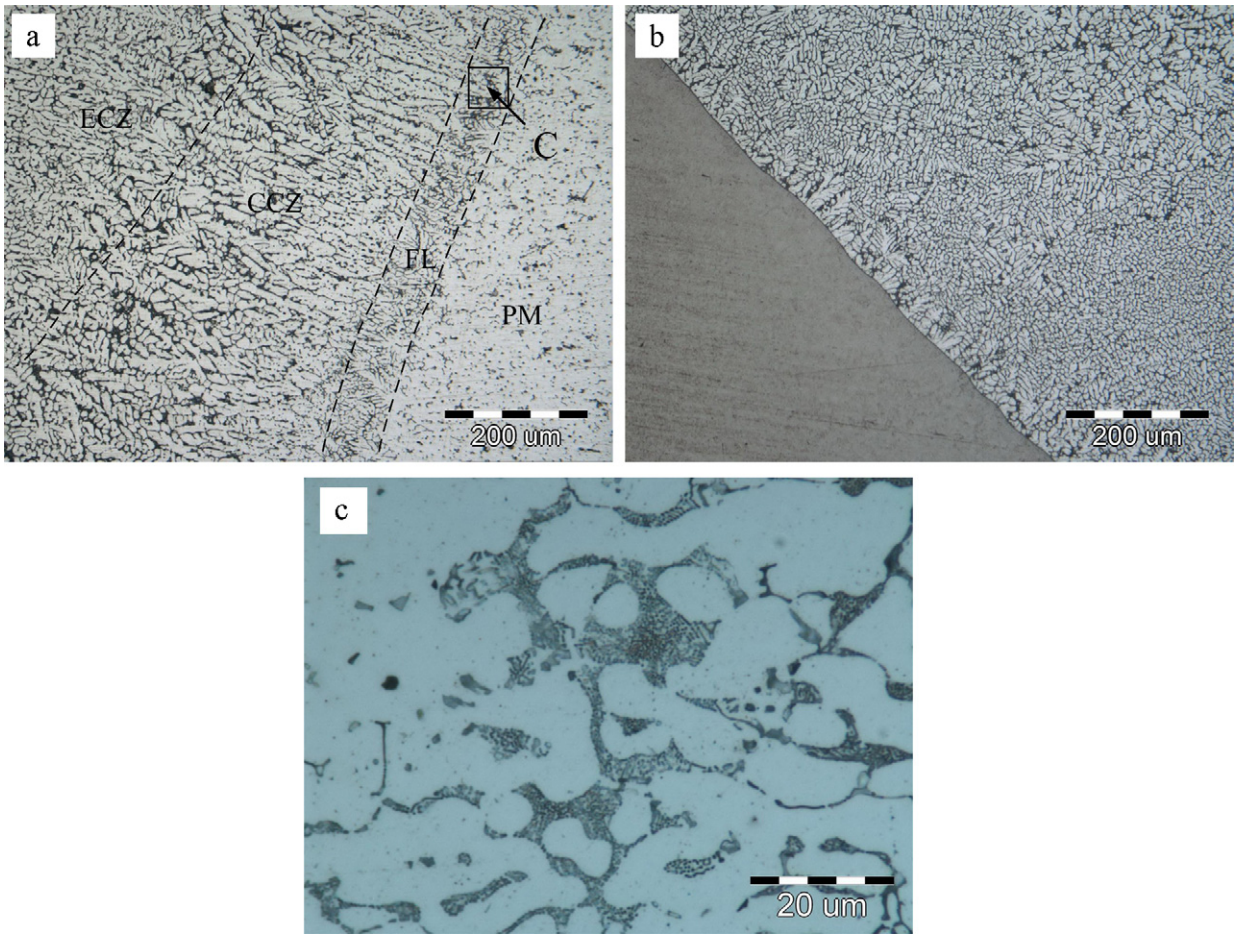

Fig. 3. Microstructure of fusion welding zone, (a) at fusion zone close to Al alloy in Fig. 2 indicated by rectangle A, (b) at fusion zone close to Ti alloy in Fig. 2 indicated by rectangle B, (c) magnified micrographs of fusion line zone in (a) indicated by rectangle C.

In order to observe the microstructure of fusion welding joint in details and identify phase structure, TEM was performed. The compound Mg_2Si was one of near-eutectic structures by selected area diffraction pattern (SADP), as shown in Fig. 4. This compound with the shape of skeleton was embedded inside α-Al grain. The Si morphology of fusion welding joint and corresponding SADP is presented in Fig. 5. According to composition between neighbouring α-Al grains by the analysis of EDS (Fig. 6), the content is very close to ternary eutectic E1 point at liquidus surface of Al–Mg–Si ternary phase diagram [29], as shown in Fig. 7. Therefore, it is confirmed that ternary near-eutectic structure is composed of compound Mg_2Si, granular Si and α-Al.

3.2. Microstructure of interfacial reaction layers

Under the condition of laser welding, interfacial reaction process is very complex due to high heating/cooling velocity. Usually, interfacial reaction mechanism is sensitive to the thermal cycle. It is implied that dynamic observation on interfacial reaction process is impossible. Thus, in order to clarify the mechanism, the phase component should be confirmed firstly and then inversion analysis will be performed. In fact, the inversion analysis method has been used frequently in the past investigations on the condition of laser heating [30].

Several layers were formed by interfacial reaction between liquid filler metal and solid Ti. The morphology observed by SEM is shown in Fig. 8. Interfacial reaction layers consist of serration-shape layer, bright thin layer and gray thin layer orderly from the seam to Ti alloy. The TEM morphology and corresponding SADP of serration-shaped reaction layer are shown in Fig. 9. According to corresponding SADP, phase of serration-shaped reaction layer was intermetallic compound $TiAl_3$.

When the thickness of reaction layer was very thin (approximately less than 1 μm), interfacial reaction layers were observed by much greater magnification, as shown in Fig. 10. Fig. 11 presents corresponding SADP of each phase in Fig. 10. It is obvious that phase structures from the seam to Ti alloy are $TiAl_3$, $Ti_7Al_5Si_{12}$, α-Ti. The layer of $Ti_7Al_5Si_{12}$ was composed of fine nanosize grains, as shown in Fig. 10(b). In addition, intermetallic compound $TiAl_3$ presents obvious crystal defect when the thickness of reaction layer is very thin, as shown in Fig. 10(c). Fig. 11(a) shows SADP that presents the fringe shape which is peculiar to stacking fault structure. Therefore, we suggest that this crystal defect is a stacking fault. Until now, the stacking fault is observed for the first time in similar conditions of interfacial reaction.

As stated above, three reaction layers composed of $TiAl_3$, $Ti_7Al_5Si_{12}$ and α-Ti are confirmed at the interface of laser welding–brazing joint.

4. Discussion

4.1. Crystallization behavior of fusion zone

According to the analysis of preceding context, microstructures of fusion welding joint were consists of α-Al grains and ternary near-eutectic structures with compound Mg_2Si, granular Si and α-

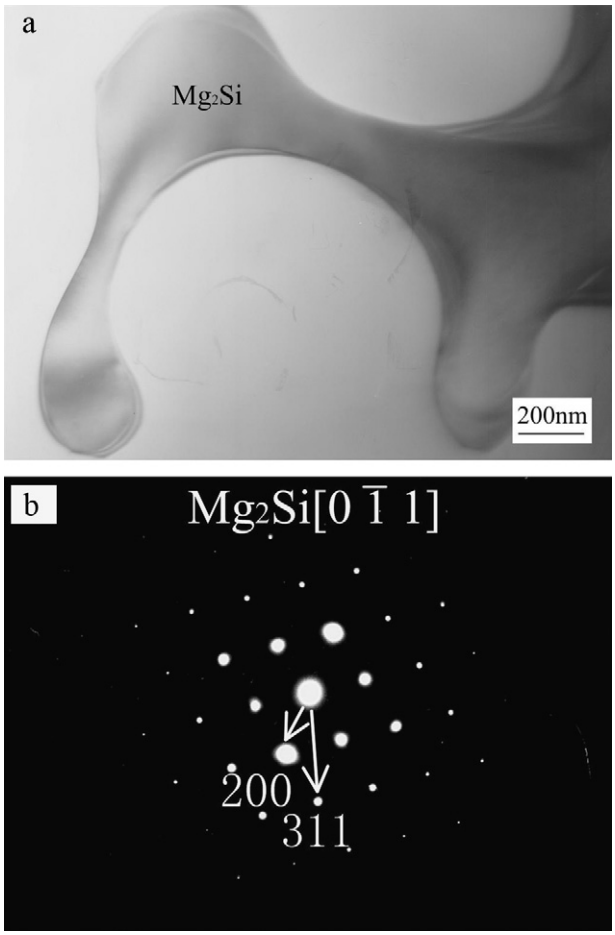

Fig. 4. Analysis of Mg_2Si in seam by TEM, (a) microstructure morphology of compound Mg_2Si, (b) SADP of compound Mg_2Si.

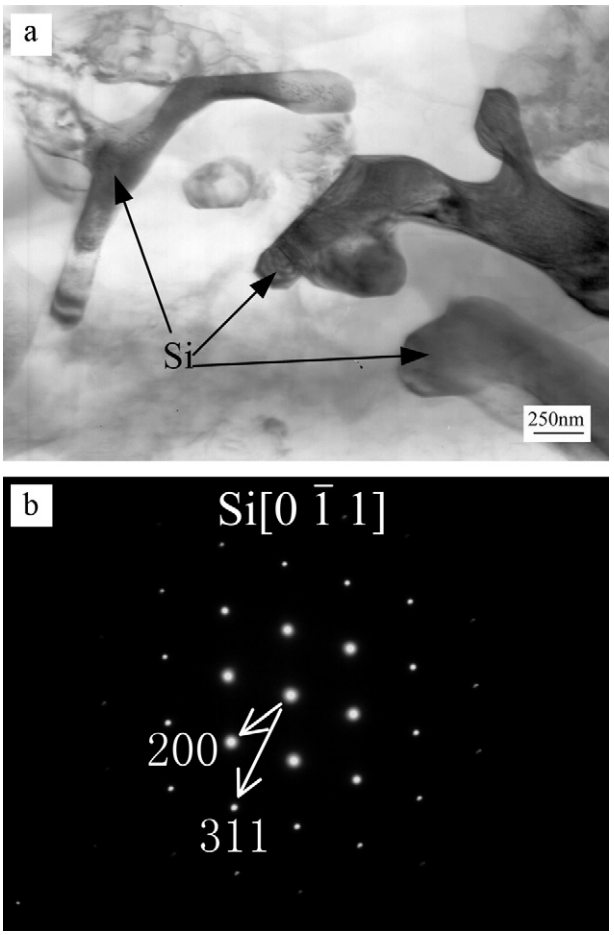

Fig. 5. Analysis of Si in the seam by TEM, (a) microstructure morphology of granular Si, (b) SADP of granular Si.

Al. Solidification process of fusion zone was described as following:

(i) During melting and mixing of filler metal and Al alloy for laser welding–brazing, only partial α-Al grains were melted in fusion line zone. In this zone, the grains have different crystal orientations depending on the ability of heat conduction. Generally, the orientation of some grains is in favor of heat conduction, and these grains were heated quickly and were melted more, whereas other grains were melted less. Thus, the metals in this zone were a semi-molten state mixed by solid and liquid metal, as shown in Fig. 12(a). At the same time, Si diffused into fusion line zone from weld pool due to the concentration gradient. As the diffusion progressed, the composition of fusion line zone approached ternary eutectic point E1 (Fig. 7). When the weld pool started to solidify, liquid metals composed of Al, Mg and Si between unfused α-Al grains started to transform to ternary near-eutectic structures with α-Al, Mg_2Si and Si. During this process, α-Al grains grew unobviously. Therefore, fine hypoeutectic microstructure was formed at FL.

(ii) With further solidifying of weld pool, α-Al grains carry out preferential heterogeneous nucleation which demands lower nucleation energy at the solid/liquid interface near Al alloy, compared with homogeneous nucleation. Along the direction perpendicular to the interface, there is the highest temperature gradient. Thus, α-Al gains grew rapidly along this direction, which induces formation of the structures with coarse columnar crystal, as shown in Fig. 12(b). During this process, a mass of Mg and Si atoms gathered between neighbouring columnar α-Al grains due to the redistribution of solutes during the solidification. Therefore, ternary near-eutectic structures with α-Al, Mg_2Si and Si were formed in this zone. In addition, in apparent columnar crystals were formed at the seam close to Ti alloy after interface reaction because thermal conductivity of Ti alloy is far lower than that of Al alloy, as shown in Fig. 12(b).

(iii) With the decreasing of the temperature, degree of supercooling increased in the weld pool. Thus, homogeneous nucleation started to proceeding and weld pool began to crystallizing. As a joining method with filler wire, weld pool was stirred sharply during the solidification. Hence, temperature distribution is more uniform than that in CCZ. Additionally, laser welding–brazing has high cooling velocity, which in weld pool induces high nucleation rate during the solidification. Therefore, a mass of fine equiaxed crystals were formed in the weld pool.

(iv) According to liquidus surface of Al–Mg–Si ternary phase diagram (Fig. 7), the compositions of the liquid metal were within hypoeutectic area. Hence, α-Al grains were precipitated from liquid phase firstly, and then the Mg and Si atoms gathered to liquid phase. The contents of Mg and Si elements between neighbouring crystallized grains increased with the growth of α-Al grains. Near-eutectic structures with Mg_2Si, Si and α-Al were formed when the contents are very close to eutectic point E1 (Fig. 7). In fact, the solidification of weld pool proceeded from bottom and both sides to upper and center on the view of macroscopic because the thermal conductivity of bottom clamping apparatus made from Cu alloy is much higher than that of upper shielding gas, as shown in Fig. 12(c). Fusion weld-

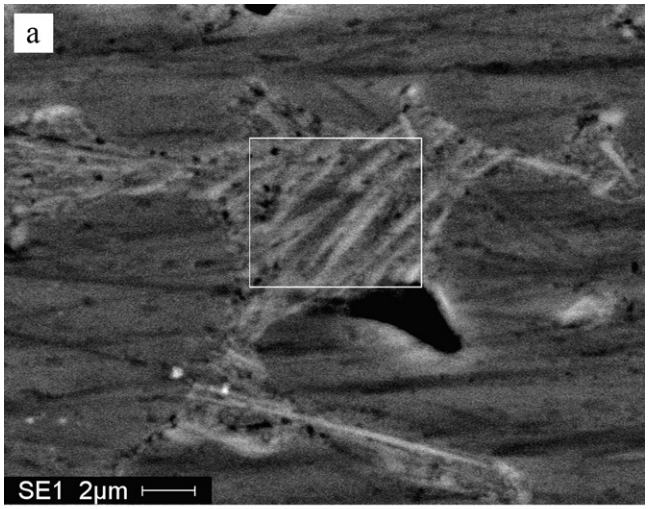

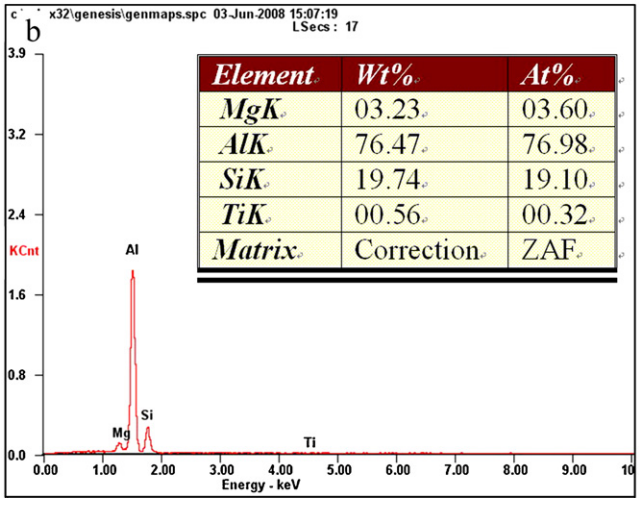

Fig. 6. EDS analysis of average composition of eutectic microstructure, (a) microstructure, (b) EDS analysis.

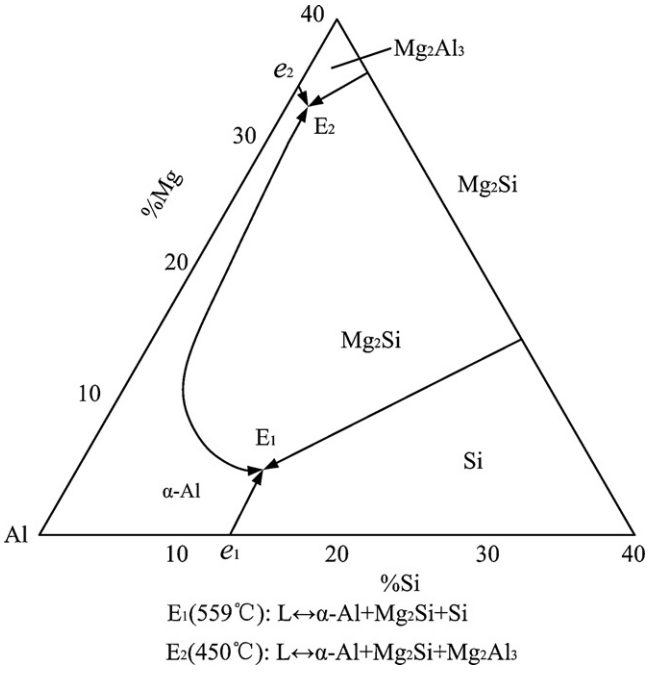

Fig. 7. Ternary phase diagram of Al–Mg–Si system.

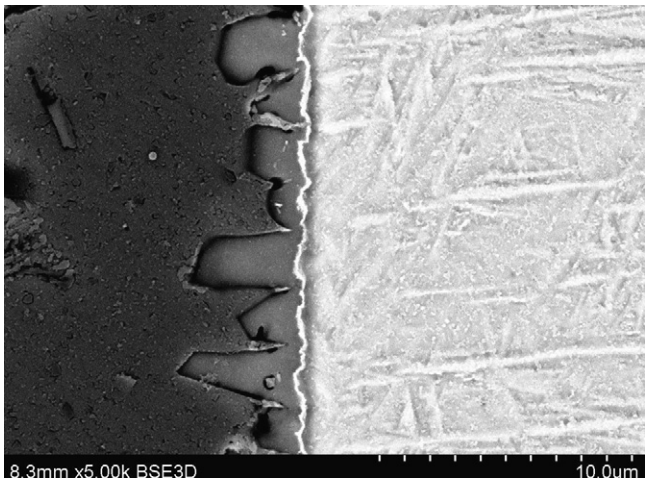

Fig. 8. Back-scattered electron morphology of interfacial reaction layer.

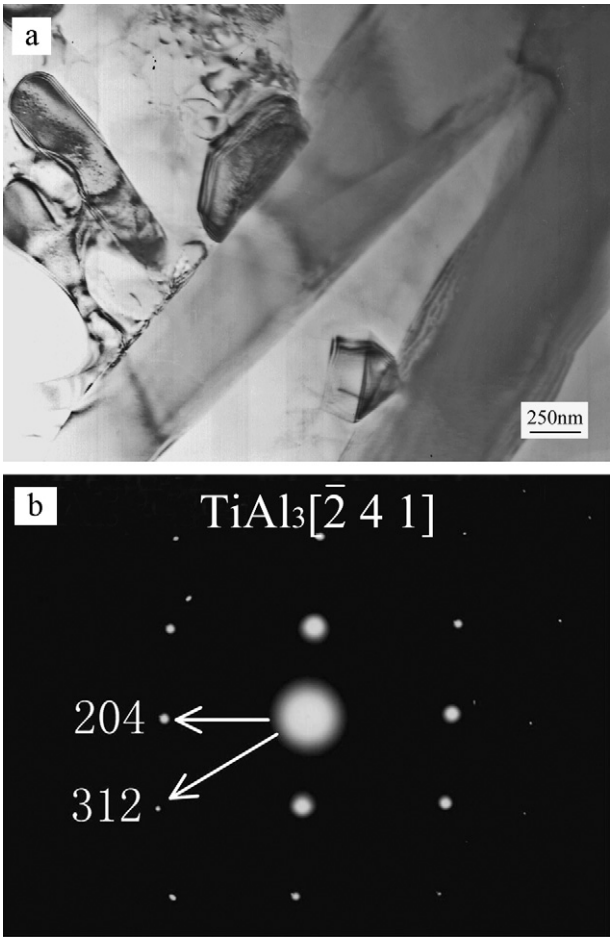

Fig. 9. Analysis of serrate-shaped intermetallic compounds by TEM, (a) microstructure, (b) SADP of $TiAl_3$

ing zone was formed after liquid metal solidifies completely, as shown in Fig. 12(d).

4.2. Mechanism of interfacial reaction

Brazing zone was formed by interfacial reaction between liquid metal and solid Ti alloy. The interfacial reaction process could be thought to occur in sequence as following:

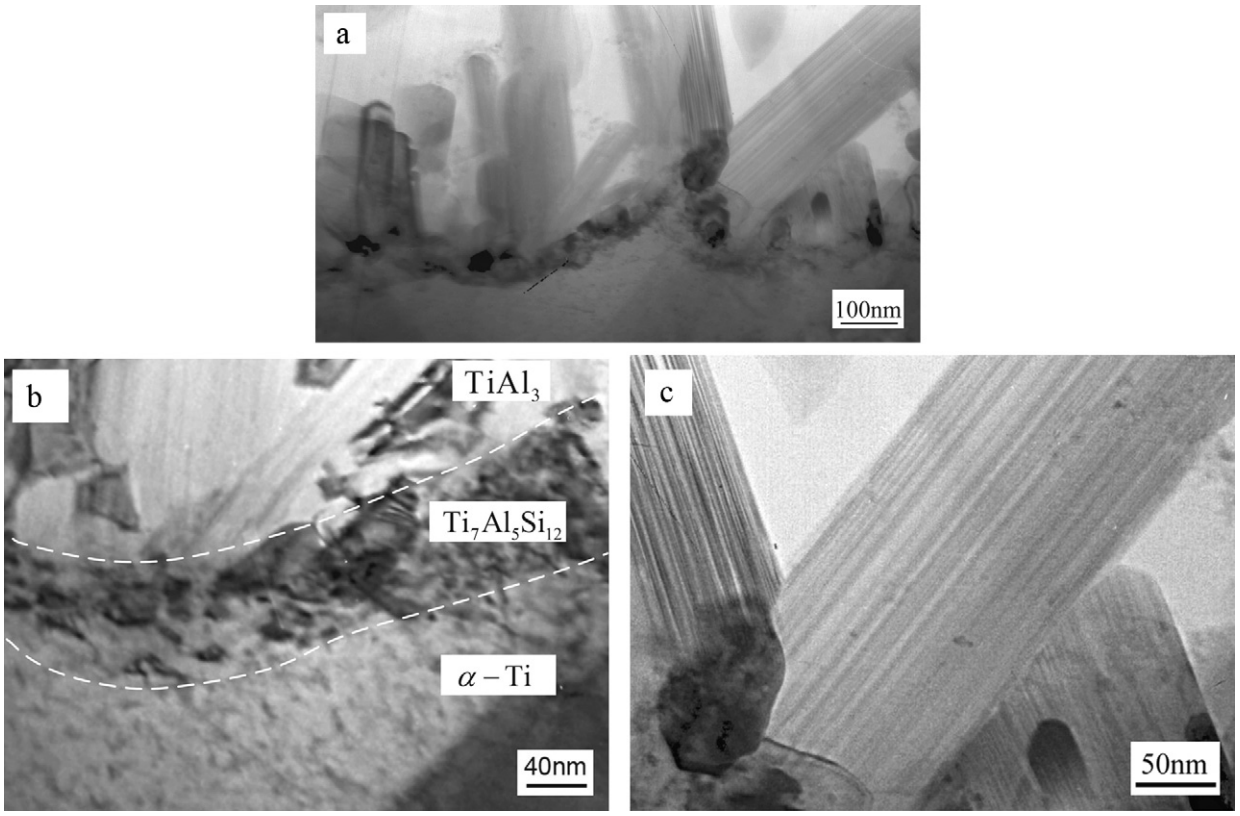

Fig. 10. Microstructure of interfacial reaction layer by TEM, (a) $TiAl_3$ morphology, (b) $Ti_7Al_5Si_{12}$ morphology, (c) fault morphology of $TiAl_3$.

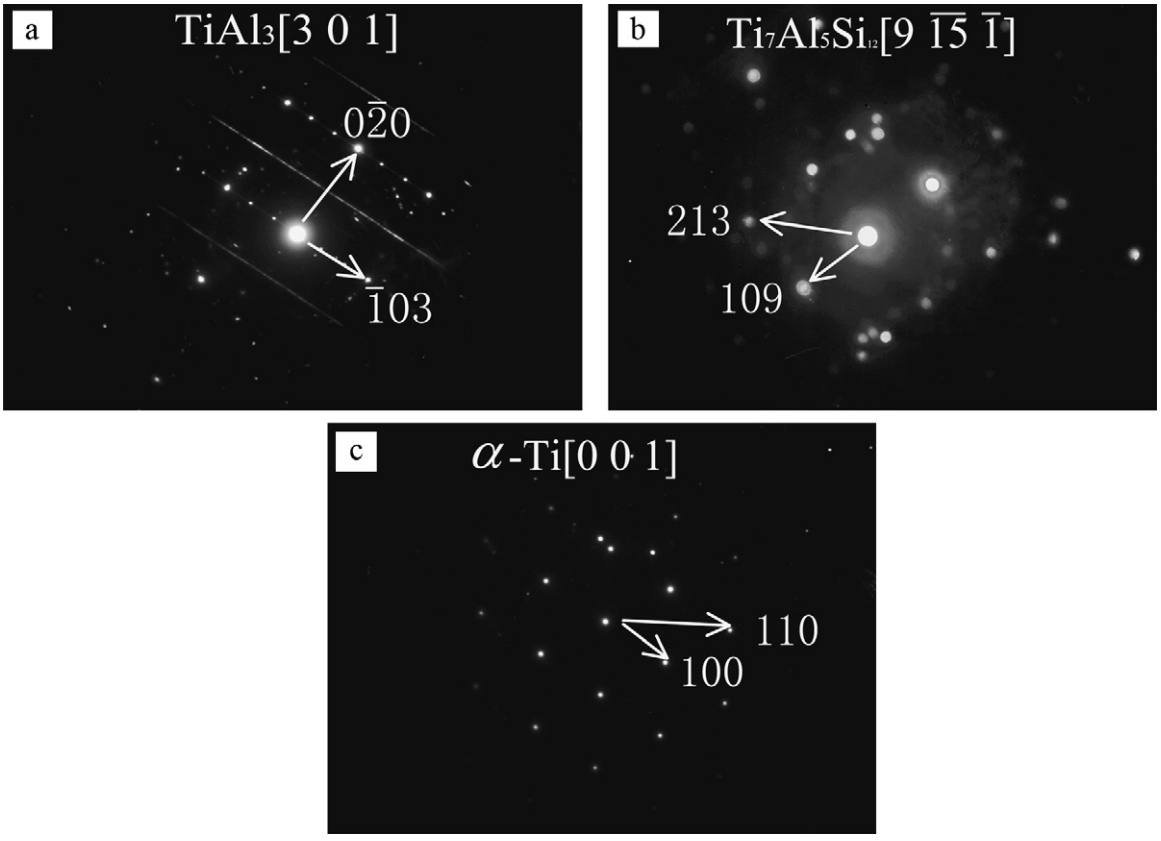

Fig. 11. Diffraction patterns of interfacial reaction layers, (a) SADP of $TiAl_3$, (b) SADP of $Ti_7Al_5Si_{12}$, (c) SADP of α-Ti.

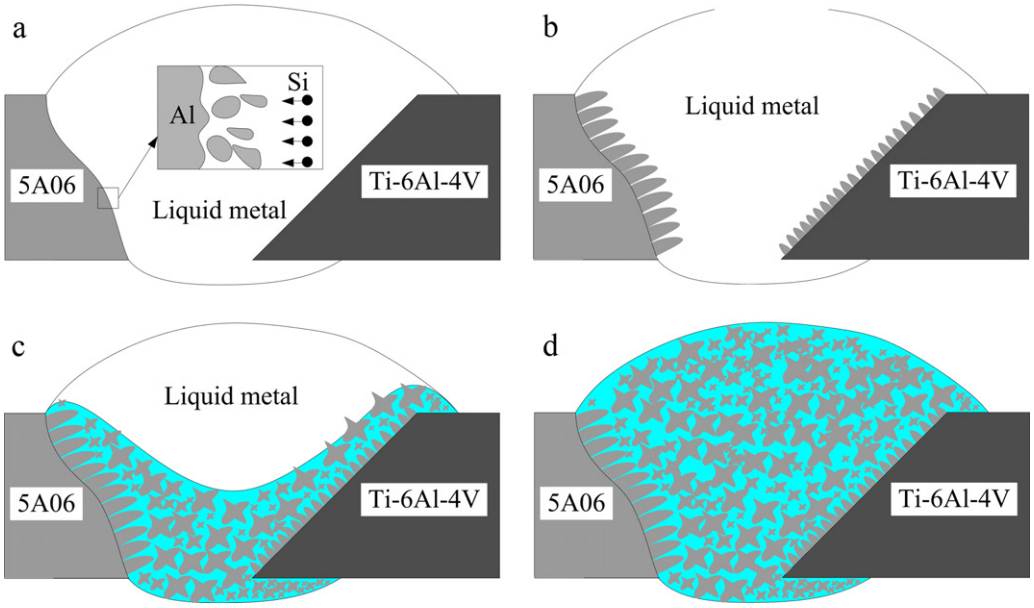

Fig. 12. Crystallization behavior of fusion welding joint, (a) formation of weld pool and diffusion of element Si, (b) formation of columnar crystal zone, (c) solidification of the seam, (d) formation of the joint.

(i) Ti–6Al–4V base metal dissolved rapidly into the liquid filler during their inchoate contact. Consequently, the Ti atoms gradually diffused from the solid/liquid interface to liquid filler as Ti alloy substrate is continuously dissolved in molten filler. In liquid filler close to the interface, the decrease of Si chemical potential was induced by the dissolution of Ti alloy. The effect of Ti dissolution on Si chemical potential was described in detail elsewhere [31]. Therefore, Si atoms continually gathered to the interface close to Ti alloy from weld pool, as shown in Fig. 13(a).

(ii) In addition, Al atoms diffused from the liquid metal to solid Ti alloy during above process, which suppress the changing from α-Ti to β-Ti, because Al is a stable element of α-Ti. So, Ti alloy close to reaction layer is generally as the form of α-Ti.

(iii) As the dissolution of Ti alloy progressed, a mass of Si atoms had gathered at the front interface in liquid metal. Accord-

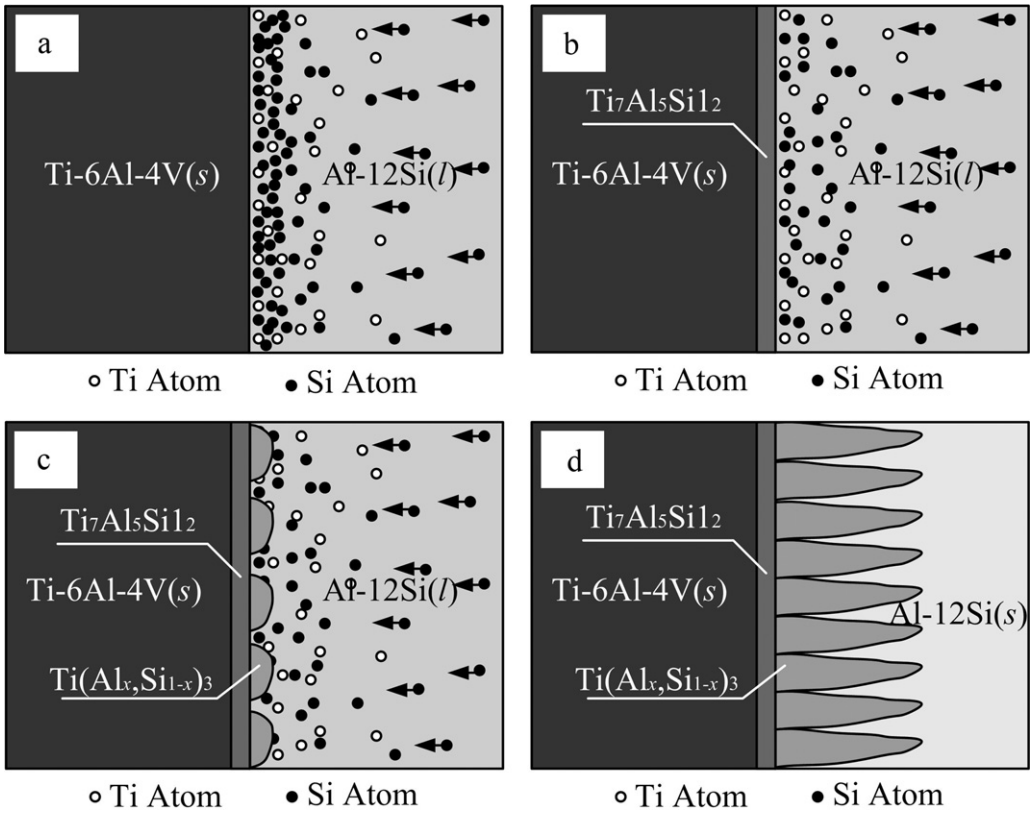

Fig. 13. Interfacial reaction mechanism of Ti/Al dissimilar alloys by laser welding–brazing for dissolution mode, (a) Dissolution of Ti alloy and segregation of Si element, (b) formation of $Ti_7Al_5Si_{12}$, (c) nucleation and growth of $TiAl_3$, (d) solidification of seam.

ing to earlier data obtained by thermodynamic calculation, the $Ti_7Al_5Si_{12}$ formation has lowest Gibbs energy change [28]. Consequently, a layer of ternary compound $Ti_7Al_5Si_{12}$ started to be formed at the interface between Ti alloy substrate and liquid metal, as shown in Fig. 13(b). The formation of $Ti_7Al_5Si_{12}$ at the interface depended on the dissolution of Ti alloy and the segregation of Si atoms. During the interfacial reaction process, Si atoms were consumed sharply, resulting in the decrease of Si content in liquid filler close to the interface. However, supplemental Ti atoms dissolved from Ti alloy and Si atoms diffused from weld pool were lower than their consumed content after the reaction of $Ti_7Al_5Si_{12}$ was performed. As a result, Si element in brazing filler metals can suppress markedly the growth of brittle reaction layer, because the dissolution of Ti alloy was weakened by the formation of ternary compound $Ti_7Al_5Si_{12}$. Moreover, compared with traditional brazing, thermal cycle of laser welding–brazing has characteristics of very short time of solid/liquid interaction and high heating/cooling velocity. This reaction process has been performed quickly due to restriction of the composition and thermal cycle. Therefore, the thickness of ternary intermetallic compound $Ti_7Al_5Si_{12}$ composed of nanosize grains was thinner.

(iv) When the contents of Ti and Si atoms in the liquid filler decreased to low enough level, intermetallic phase $TiAl_3$ began to crystallize at the interface. Heterogeneous nucleation was achieved easily at solid/liquid interface, as shown in Fig. 13(c). In general, intermetallic compound with ordered structure has preferred orientation during its crystallization process, which induces the formation of serration-shaped reaction layer, as shown in Fig. 13(d). During $TiAl_3$ growing, Si element still gathered toward the interface, and up to 15 at.%Al can be replaced by Si in $TiAl_3$ lattice structures due to the similar atomic radii and it can be written as $Ti(Al,Si)_3$ [32,33]. In addition, $TiAl_3$ reaction layer with stacking fault structure may be induced by complicated stress state during the progress of interfacial reaction.

5. Conclusions

According to the study on joining mechanism of the joint by laser welding–brazing of Ti/Al dissimilar alloys, conclusions were summarized as follows:

(1) The fusion welding zones are divided into fusion line (FL), columnar crystal zone (CCZ) and equiaxed crystal zone (ECZ). The microstructures of welding joint consist of α-Al grains and ternary near-eutectic structure including α-Al, Si and Mg_2Si.

(2) Fusion line with fine hypoeutectic microstructure was formed by diffusion of element Si from weld pool to semi-molten zone at solid/liquid interface. The columnar crystal was formed due to obvious directionality of heat conduction. Equiaxed crystals were formed in the weld pool due to the stir by filler wire and high degree of supercooling.

(3) The microstructures of brazing zone are orderly from Ti alloy to the seam consists of α-Ti, nanosize granular $Ti_7Al_5Si_{12}$ and serration-shaped $TiAl_3$. Apparent stacking fault structure of intermetallic compound $TiAl_3$ was found.

(4) During the interfacial reaction at solid/liquid interface, the formation of $Ti_7Al_5Si_{12}$ depended on the dissolution of Ti alloy and the segregation of Si atoms, and intermetallic phase $TiAl_3$ was formed by the crystallization. Growth of brittle reaction layer could be suppressed because dissolution of Ti alloy was weakened by formation of ternary compound $Ti_7Al_5Si_{12}$.

Acknowledgments

The authors would like to thank State Key Laboratory of Welding of China, all of the work within which were conducted. They also appreciate the financial support from the National Natural Science Foundation of China (No. 51004009).

References

[1] A.N. Alhazaa, T.I. Khan, J. Alloys Compd. 494 (2010) 351–358.
[2] A.S. Ramos, M.T. Vieira, J. Morgiel, J. Grzonka, S. Simões, M.F. Vieira, J. Alloys Compd. 484 (2009) 335–340.
[3] J.W. Ren, Y.J. Li, T. Feng, Mater. Lett. 56 (2002) 647–652.
[4] T. Saeid, A. Abdollah-zadeh, B. Sazgari, J. Alloys Compd. 490 (2010) 652–655.
[5] A. Abdollah-Zadeh, T. Saeid, B. Sazgari, J. Alloys Compd. 460 (2008) 535–538.
[6] Won-Bae Lee, Kuek-Saeng Bang, Seung-Boo Jung, J. Alloys Compd. 390 (2005) 212–219.
[7] J.L. Song, S.B. Lin, C.L. Yang, C.L. Fan, J. Alloys Compd. 488 (2009) 217–222.
[8] A. Elrefaey, W. Tillmann, J. Alloys Compd. 487 (2009) 639–645.
[9] W.H. Sohn, H.H. Bong, S.H. Hong, Mater. Sci. Eng. A 355 (2003) 231–240.
[10] M. Kreimeyer, F. Wagner, F. Vollertsen, Opt. Laser. Eng. 43 (2005) 1021–1035.
[11] A. Mathieu, S. Pontevicci, J.C. Viala, E. Cicala, S. Matteï, D. Grevey, Mater. Sci. Eng. A 435–436 (2006) 19–28.
[12] W.V. Vaidya, M. Horstmann, V. Ventzke, B. Petrovski, M. Kocak, R. Kocik, G. Tempus, Mat.-Wiss. u Werkstofftech 40 (2009) 623–633.
[13] W.V. Vaidya, M. Horstmann, V. Ventzke, B. Petrovski, M. Kocak, R. Kocik, G. Tempus, Mat.-Wiss. u Werkstofftech 40 (2009) 769–779.
[14] N. Kahraman, B. Gulenc, F. Findik, Int. J. Impact Eng. 34 (2007) 1423–1432.
[15] T. Takemoto, I. Okamoto, J. Mater. Sci. 23 (1988) 1301–1308.
[16] Y.C. Chen, K. Nakata, Mater. Des. 30 (2009) 469–474.
[17] H.S. Wang, H.G. Chen, J.S.C. Jang, J. Alloys Compd. 495 (2010) 224–228.
[18] H. Yan, A.H. Wang, K.D. Xu, W.Y. Wang, Z.W. Huang, J. Alloys Compd. 505 (2010) 645–653.
[19] C.G. Li, Y. Wang, L.X. Guo, J.Q. He, Z.Y. Pan, L. Wang, J. Alloys Compd. 506 (2010) 356–363.
[20] X.B. Liu, G. Yu, J. Guo, Y.J. Gu, M. Pang, C.Y. Zheng, H.H. Wang, J. Alloys Compd. 453 (2008) 371–378.
[21] X.B. Liu, M. Pang, J. Guo, G. Yu, J. Alloys Compd. 461 (2008) 648–653.
[22] H. Laukant, C. Wallmann, M. Korte, U. Glatzel, Adv. Mater. Res. 6–8 (2005) 163–170.
[23] K. Saida, W. Song, K. Nishimoto, Sci. Technol. Weld. Joint 10 (2005) 227–235.
[24] R. Borrsutthekul, T. Yachi, Y. Miyashita, Y. Mutoh, Mater. Sci. Eng. A 467 (2007) 108–113.
[25] G. Sierra, P. Peyre, F. Deschaux Beaume, D. Stuart, G. Fras, Mater. Charact. 59 (2010) 1705–1715.
[26] Y.B. Chen, S.H. Chen, L.Q. Li, Int. J. Adv. Manuf. Technol. 44 (2009) 265–272.
[27] Y.B. Chen, S.H. Chen, L.Q. Li, Mater. Des. 31 (2010) 227–233.
[28] S.H. Chen, L.Q. Li, Y.B. Chen, Mater. Sci. Technol. 26 (2010) 230–235.
[29] D.L. Hu, F. Zhang, Phase Diagrams of Ternary Alloy, Northwestern Polytechnical University Press, Xi'an, 1995.
[30] Y.B. Chen, D.J. Liu, L.Q. Li, F.Q. Li, J. Alloys Compd. 484 (2009) 108–112.
[31] S.H. Chen, L.Q. Li, Y.B. Chen, D.J. Liu, Trans. Nonferrous Met. Soc. China 20 (2010) 64–70.
[32] C.R.F. Azevedo, H.M. Flower, Mater. Sci. Technol. 16 (2000) 372–381.
[33] M. Zeren, E. Karakulak, J. Alloys Compd. 450 (2008) 255–259.